

$A\text{Fe}_2\text{As}_2$ ($A = \text{Ca}, \text{Sr}, \text{Ba}, \text{Eu}$) and $\text{SrFe}_{2-x}\text{TM}_x\text{As}_2$ ($\text{TM} = \text{Mn}, \text{Co}, \text{Ni}$): crystal structure, charge doping, magnetism and superconductivity

Deepa Kasinathan,¹ Alim Ormeci,¹ Katrin Koch,¹ Ulrich
Burkhardt,¹ Walter Schnelle,¹ Andreas Leithe-Jasper,¹ Helge
Rosner¹

¹Max-Planck-Institut für Chemische Physik fester Stoffe, Dresden, Germany

E-mail: Deepa.Kasinathan@cpfs.mpg.de, Rosner@cpfs.mpg.de

Abstract. The electronic structure and physical properties of the pnictide compound families REOFeAs ($\text{RE} = \text{La}, \text{Ce}, \text{Pr}, \text{Nd}, \text{Sm}$), $A\text{Fe}_2\text{As}_2$ ($A = \text{Ca}, \text{Sr}, \text{Ba}, \text{Eu}$), LiFeAs and FeSe are quite similar. Here, we focus on the members of the $A\text{Fe}_2\text{As}_2$ family whose sample composition, quality and single crystal growth are better controllable compared to the other systems. Using first principles band structure calculations we focus on understanding the relationship between the crystal structure, charge doping and magnetism in $A\text{Fe}_2\text{As}_2$ systems. We will elaborate on the tetragonal to orthorhombic structural distortion along with the associated magnetic order and anisotropy, influence of doping on the A site as well as on the Fe site, and the changes in the electronic structure as a function of pressure. Experimentally, we investigate the substitution of Fe in $\text{SrFe}_{2-x}\text{TM}_x\text{As}_2$ by other $3d$ transition metals, $\text{TM} = \text{Mn}, \text{Co}, \text{Ni}$. In contrast to a partial substitution of Fe by Co or Ni (electron doping) a corresponding Mn partial substitution does not lead to the suppression of the antiferromagnetic order or the appearance of superconductivity. Most calculated properties agree well with the measured properties, but several of them are sensitive to the As z position. For a microscopic understanding of the electronic structure of this new family of superconductors this structural feature related to the Fe-As interplay is crucial, but its correct ab initio treatment still remains an open question.

Submitted to: *New J. Phys.*

1. Introduction

Physics community around the world has been tirelessly working for the past months to find different ways of increasing the superconducting transition temperature T_c following the discovery of superconductivity at 26 K in the rare-earth based (*RE*OFeAs) system LaO_{1-x}F_xFeAs ($x = 0.05 - 0.12$) [1]. Spirited search by the experimentalists has led to eventually raising T_c to 55 K for another member of this family of compounds, SmFeAsO_{0.9}F_{0.1} [2]. Shortly afterwards, another family of Fe-based compounds AFe₂As₂ ($A = \text{Ca, Sr, Ba, Eu}$) was also found to be superconducting upon hole doping [3] on the *A* site with a maximum $T_c = 38$ K [4, 5, 6]. These discoveries are followed by the announcements of other new parent compounds: LiFeAs, FeSe, SrFeAsF with a maximum T_c of 18 K [7], 14 K [7] (27 K using pressure [8]) and 56 K [9], respectively. The basic features, that are common to many of these new parent compounds, are the anti-ferromagnetic ordering of the Fe-spins at $T_N \approx 100\text{--}200$ K, and the quasi-2D nature of the electronic structure. All the members belonging to the above mentioned families have been shown to superconduct upon either “hole” or “electron doping” only with the exception of LiFeAs, wherein it is considered that the Li layer acts as a charge reservoir for the system [7]. Superconductivity also emerges upon application of hydrostatic pressure for certain members of the *RE*OFeAs, AFe₂As₂ and FeSe families. Notwithstanding the abundant research that has already been performed, the microscopic nature of the mechanism of superconductivity has thus far remained elusive. A systematic study of the many members within one particular family, using both experimental and theoretical techniques, would pave way to a more concrete understanding of the electronic structure of the normal state. Although the *RE*OFeAs systems have larger T_c values, their sample preparation, characterization and quality, as is the case for many oxides, have to be considered with great care. Alternatively it has been demonstrated that the AFe₂As₂ systems could be synthesized comparatively easier. Consequently, here we carry out a systematic investigation using both theoretical and experimental techniques for the AFe₂As₂ systems.

All the AFe₂As₂ compounds crystallize in the tetragonal ThCr₂Si₂-type structure at room temperature. They all exhibit a structural transition upon cooling to an orthorhombic lattice (T_0 for Ca ≈ 171 K [10], Sr ≈ 205 K [11], Ba ≈ 140 K [12], Eu ≈ 200 K [13]). The structural transition is coupled with an antiferromagnetic ordering of the Fe moments with a wave vector $Q = [1,0,1]$ for the spin-density-wave (SDW) pattern. Suitable substitution on either the *A* site or the Fe site can suppress the magnetic ordering, and then the system becomes superconducting for certain ranges of doping (for example, maximum $T_c = 38$ K (Ba,K)Fe₂As₂ [6], 32 K (Eu,K)Fe₂As₂ [14], 21 K Sr(Fe,Co)₂As₂ [15], Ba(Fe,Co)₂As₂ [16]). Superconductivity can also be induced in “undoped” and “under-doped” compounds by applying pressure [17].

In the following sections we describe the microscopic picture of the magneto-structural transition and the effects of external pressure, chemical pressure and charge doping on the AFe₂As₂ systems. In order to make the manuscript more easily readable,

we introduce the following abbreviations: *REOF*eAs: 1111, *AFe₂As₂*: 122, *LiFeAs*: 111, *FeSe*: 11, *SrFeAsF*: 1111'; ferromagnetic: FM, checkerboard (nearest neighbour) antiferromagnetic: NN-AFM, columnar/stripe-type antiferromagnetic order of the Fe-spins: SDW (spin-density-wave).

2. Methods

2.1. Theory

We have performed density functional band structure calculations using a full potential all-electron local orbital code FPLO [18, 19, 20] within the local (spin) density approximation (L(S)DA) including spin-orbit coupling when needed. The Perdew-Wang [21] parametrization of the exchange-correlation potential is employed. Density of states (DOS) and band structures were calculated after converging the total energy on a dense *k*-mesh with 24×24×24 points. The strong Coulomb repulsion in the Eu 4*f* orbitals are treated on a mean field level using the LSDA+*U* approximation in the atomic-limit double counting scheme [22]. Results we present below use the LSDA+*U* method [23] in the rotationally invariant form [24]. In accordance with the widespread belief that in the new Fe-based superconducting compounds the Fe 3*d* electrons have a more itinerant character than a localized one, and thereby are much less correlated in comparison to the Cu 3*d* electrons in the high-*T_c* cuprates, we did not apply the LSDA+*U* approximation to the Fe 3*d* states. Effects of doping on either the cation site or the Fe site were studied using the virtual crystal approximation (VCA) treatment. The results obtained via VCA were cross checked using supercells for certain doping concentrations. The crystal structures are optimized at different levels to investigate or isolate effects that may depend sensitively to certain structural features. The full relaxation of the unit cell of the 122 systems at low temperatures involves optimizing *a/b* and *c/a* ratios in addition to relaxing the As-*z* position.

2.2. Experimental

Polycrystalline samples were prepared by sintering in glassy-carbon crucibles which were welded into tantalum containers and sealed into evacuated quartz tubes for heat treatment at 900°C for 16 hours with two regrinding and compaction steps. First precursors SrAs, Co₂As, Fe₂As, Mn₂As and NiAs were synthesized from elemental powders sintered at 600°C for 48 h (Mn, Fe, Co, Ni 99.9 wt.%; As 99.999 wt.%; Sr 99.99 wt.%). These educts were powdered, blended in stoichiometric ratios, compacted to pellets, and heat treated. All sample handling was done inside argon-filled glove boxes. Crystals were grown in glassy-carbon crucibles by a modified self flux method [25, 16] in melts with compositions SrFe_{5-*x*}Co_{*x*}As₅ (0.5 ≤ *x* ≤ 0.85) by cooling from 1250°C to 1100°C within 48 hours. The melt was spun off at 1100°C using a centrifuge [26]. Metallographic investigations were performed on polished surfaces of selected secured crystal platelets. Electron-probe microanalysis (EPMA) with wavelength-

dispersive analysis was accomplished in a Cameca SX100 machine. Crystal X1 was grown in a flux SrFe_{4.25}Co_{0.75}As₅ and crystal X2 in a flux SrFe_{0.15}Co_{0.85}As₅. For crystal X1 from EPMA the composition (in at.%) Sr_{19.9(2)}Fe_{36.2(1)}Co_{4.2(1)}As_{39.7(1)} was found which corresponds to SrFe_{2-x}Co_xAs₂ with $x \approx 0.21$. For crystal X2 from EPMA the composition (in at.%) Sr_{19.5(2)}Fe_{35.5(1)}Co_{5.0(2)}As_{39.9(2)} was found which corresponds to SrFe_{2-x}Co_xAs₂ with $x \approx 0.25$. Crystals grown from a flux SrFe_{4.5}Co_{0.5}As₅ had a composition of Sr_{19.9(3)}Fe_{36.9(1)}Co_{3.2(1)}As_{39.9(2)} corresponding to SrFe_{2-x}Co_xAs₂ with $x \approx 0.15$ and showed no superconductivity. All crystals grown up to now exhibit some inclusions of flux-material which can be seen in Fig. 1 (for crystal X2 the second phase has the composition Sr₃₍₁₎Fe₄₄₍₁₎Co₈₍₁₎As₄₅₍₁₎ (in at.%)).

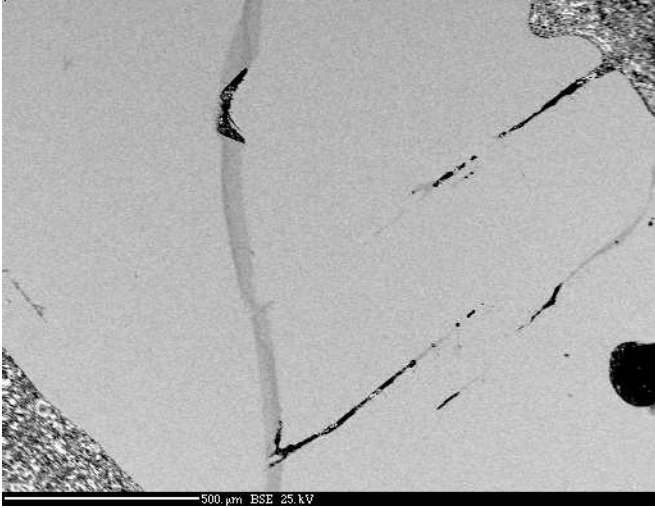


Figure 1. Micrograph of a polished crystal from the same batch crystal X2 was selected. Light grey phase: bulk crystal. Dark grey phase: inclusions of flux. Black regions: micro-cracks and cavities.

3. Results - Theory

3.1. Ambient-temperature phase : tetragonal

We begin with comparing the DOS computed for a representative member of each family of the iron pnictide compounds. In these calculations, experimental values of the ambient-temperature tetragonal lattice parameters and atomic positions were used for all the systems. Collected in Fig. 2 are the non-magnetic total and orbital-resolved DOS for five systems: 1111, 122, 111, 11, 1111'. The states close to the Fermi energy (E_F) in all these systems are comprised mainly of Fe 3d contributions. The contribution of the pnictide atom (or Se in the case of FeSe) to the Fermi surface is small but non-zero. A pseudo-gap-like feature in the DOS slightly above the E_F is common to all the systems. At the outset, all the five systems look quite similar to one another, but slight differences are already visible when analyzing the Fe 3d orbital resolved DOS, presented on right panels in Fig. 2. The contribution of the Fe 3d_{x²-y²} orbital (the orbital pointing directly towards the nearest neighbour Fe ions) is the largest close to E_F for all the systems. The corresponding bands (not shown here) are highly dispersive in the $a - b$ plane and

remain flat along the c -axis, indicative of the quasi-2D nature of this band. The distance of the $3d_{x^2-y^2}$ edge from the E_F varies for the different systems and is the largest for the 111 family and smallest for the 1111 family. The second largest contribution to the Fermi surface comes from the doubly degenerate $3d_{xz}$ and $3d_{yz}$ orbitals and this feature is again consistent for all the iron pnictide compounds.

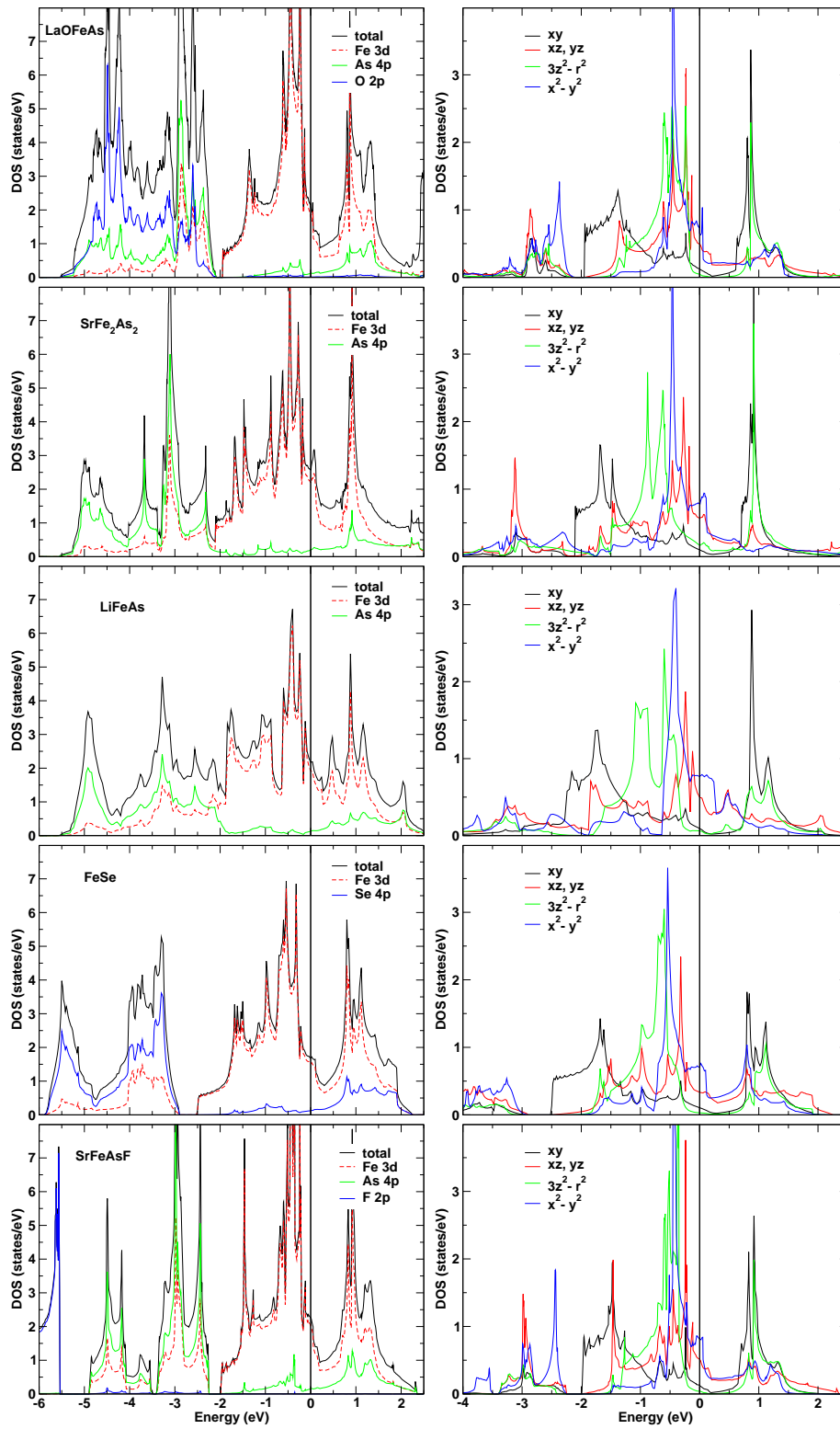


Figure 2. Comparison of total and site-resolved density of states (DOS) per cell (left panel) and Fe 3d orbital resolved DOS (right panel) of a representative member for each of the new superconducting family of compounds. LaOFeAs:1111, SrFe₂As₂:122, LiFeAs:111, FeSe:11, SrFeAsF:1111'. The solid vertical lines at zero energy denote the Fermi level E_F .

3.2. Structural distortion vs. magnetic order

3.2.1. Tetragonal to orthorhombic distortion As discussed above, the FeAs-based compounds crystallizing in different structures have very similar electronic properties. However, between the 1111 and the 122 families there is an important difference in regard to structural and magnetic transitions. In the former, the transition temperatures for the structural transition are 10–20 K higher than those of the magnetic one. On the other hand, for the 122 family the structural and the magnetic transitions are found to be coupled and occur at the same temperature. By first-principles calculations we explored the nature of this intimate connection between the two transitions for the 122 systems.

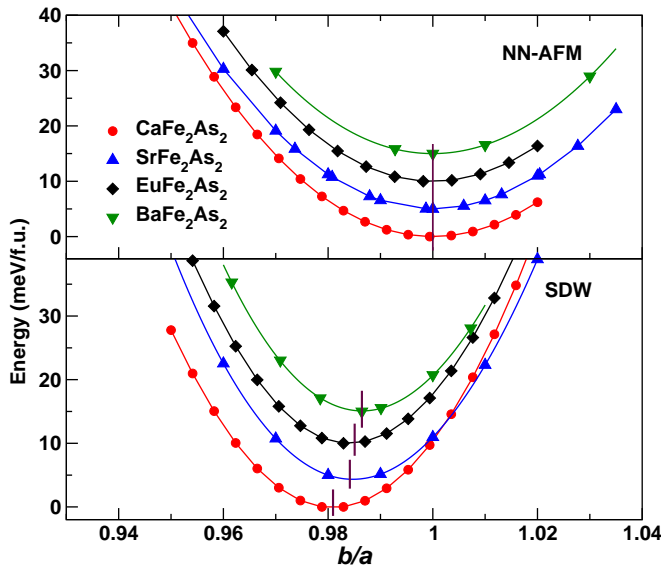


Figure 3. Total energy as a function of b/a for the $A\text{Fe}_2\text{As}_2$ ($A = \text{Ca}, \text{Sr}, \text{Eu}, \text{Ba}$) systems with two possible spin arrangements between the Fe spins. In NN-AFM the spins of all the nearest neighbours are anti-parallel to each other. In the SDW pattern, the spins along the longer a -axis are anti-parallel while the spins along the shorter b -axis are parallel. The solid vertical lines denote the minimum value of the energy. The minimum energy for each system has been set to zero. For clarity, Sr122, Eu122 and Ba122 curves are offset by 5, 10 and 15 meV.

Table 1. Comparison of b/a obtained from LSDA for the SDW pattern with experimental reports. The references from which the experimental numbers are obtained are indicated. With the exception of Ca122, (more detailed discussion, see text) the trend in the in-plane axis distortion for the orthorhombic structure is consistent with experimental findings.

	b/a -LSDA	b/a -expt	Ref
Ca122	0.9809	0.9898	[27]
Sr122	0.9841	0.9889	[28]
Eu122	0.9850	0.9898	[29]
Ba122	0.9864	0.9928	[12]

We calculated total energies for different b/a ratios for different magnetic models. For the nonmagnetic (NM), ferromagnetic (FM) (not shown) as well as the nearest-neighbour antiferromagnetic (NN-AFM) (Fig. 3, upper panel) patterns, lowest total

energy occurred at $a = b$, indicating that for these patterns the tetragonal structure is more stable than the orthorhombic structure. Inclusion of spin-orbit effects did not change this result. The tetragonal to orthorhombic distortion is obtained only for the SDW pattern as displayed in the lower panel of Fig. 3. Hence, LSDA calculations clearly show that the SDW state is necessary for the tetragonal-to-orthorhombic transition to take place. The size of this effect, namely the deviation of the calculated b/a ratio from unity, depends on the size of the cation, the ratio being smallest in BaFe₂As₂, and largest in CaFe₂As₂. The values obtained via LSDA are collected in Table 1 and compared to the experimental reports. The trend obtained in LSDA fits well with the experimental b/a ratios with the exception of CaFe₂As₂. Experimentally, CaFe₂As₂ crystals are shown to have complex microstructure properties. Recent studies using transmission electron microscopy (TEM) [30] have shown a pseudo-periodic modulation and structural twinning arising from tetragonal to orthorhombic transition only in CaFe₂As₂ but not in Sr or Ba 122 systems. A structural twinning hinders the correct estimation of the lattice parameters and thereby may explain the experimental deviation in the trend of b/a ratio for CaFe₂As₂ with respect to LSDA.

In all four compounds the coupling along the shorter in-plane axis is FM in agreement with experimental findings. Although these results are robust with respect to details of structure and calculations, the preferred direction of the spins are found to be quite sensitive. We performed fully-relativistic calculations for $A = \text{Ca, Sr and Ba}$ cases using (i) SDW with $Q = [1\ 0\ 0]$, (ii) SDW with $Q = [1\ 0\ 1]$. The latter SDW pattern requires the doubling of the c lattice parameter and the corresponding calculations are highly time consuming. Therefore, only the cartesian axes are considered for possible spin orientations, and the structural data corresponding to the minima in Fig. 3 are used. In the Sr122 case for both SDW patterns we find the direction of the AFM coupling (along the longer a -axis) as the easy axis in agreement with the neutron scattering study result [28]. However, in Ca and Ba 122 cases different axes in the (a, b) plane are found as easy axes for different SDW patterns. The longer a -axis, is the easy axis for Ba (Ca) 122 for $Q = [1\ 0\ 0]$ ($Q = [1\ 0\ 1]$); the shorter axis, b , the direction of FM coupling, for Ba (Ca) 122 for $Q = [1\ 0\ 1]$ ($Q = [1\ 0\ 0]$). Since the involved energy differences are tiny (of the order of 15–30 μeV per atom), a satisfactory resolution of this issue requires further study. Experimental study on Ba122 [31] has been able to determine that spins lie along the longer a -axis.

3.2.2. Plasma frequency and effective dimensionality Band structure calculations can provide information on the “effective dimensionality” in a compound through various means, such as dispersionless (flat) energy bands along certain symmetry lines, van Hove singularities in DOS, etc. A simple quantitative measure, however, can be obtained by computing plasma frequencies along the main unit cell axes. For all of the 122 compounds as well as the representative compounds for the other families, plasma frequencies are calculated by nonmagnetic calculations using the experimental structural data of the tetragonal phase. In Table 2 we present the ratio

Table 2. Ratio of the in-plane plasma frequency ω_p^a to the out-of-plane plasma frequency ω_p^c for various members of the Fe-based superconducting systems. The observed trend in the plasma frequency ratios follows the trend in the ratios of the (inter-layer to intra-layer) Fe-Fe distances, $d_c^{\text{Fe-Fe}}/d_a^{\text{Fe-Fe}}$. As we go down the column, the systems go from being more 2D towards being more 3D. The maximum superconducting transition temperature T_c^{max} obtained either via doping or pressure is also collected in the last column. The trend in T_c^{max} also follows the trend in ω_p^a/ω_p^c , with decreasing temperatures when the systems become more 3D.

	ω_p^a/ω_p^c	c/a	$d_c^{\text{Fe-Fe}}/d_a^{\text{Fe-Fe}}$	T_c^{max} (K)
SrFeAsF	19.892	2.2426	3.1715	56 [9]
LaOFeAs	8.9467	2.1656	3.0626	55 [2]
FeSe	4.1119	1.4656	2.0727	27 [8]
LiFeAs	3.2181	1.6785	2.3738	18 [7]
BaFe ₂ As ₂	3.2926	3.2850	2.3228	38 [6]
SrFe ₂ As ₂	2.8329	3.1507	2.2279	38 [5, 4]
CaFe ₂ As ₂	1.3953	3.0287	2.1416	20 [32]

of the in-plane plasma frequency ($\omega_p^a = \omega_p^b$) to the plasma frequency along the c -axis (ω_p^c). One notices that for the 122 family the results are in line with expectations: the compound is least anisotropic (more 3D-like) for the smallest cation (Ca), and strongly anisotropic (less 3D-like) for the largest cation (Ba). Additionally, the 1111 and 1111' families are seen to be much more anisotropic (more 2D-like) than all of the others.

In the case of iron arsenides, in a rather simplified picture, one expects the plasma frequency ratio to be proportional to the ratio of the shortest interlayer ($d_c^{\text{Fe-Fe}}$) to the shortest intralayer Fe-Fe distances ($d_a^{\text{Fe-Fe}}$). In terms of lattice parameters the distance ratio $d_c^{\text{Fe-Fe}}/d_a^{\text{Fe-Fe}}$ is $c/\sqrt{2}a$ for 122's and $\sqrt{2}c/a$ for the others. Table 2 shows that these two ratios are largely correlated with apparently the exception of FeSe [33].

3.2.3. Effect of the As z position and magnetic moments from LDA: In any first-principles study of a magnetic system, an essential aspect is the comparison of the computed magnetic moments with the experimentally deduced ones. This standard procedure proves to be quite tricky in these FeAs-based compounds due to the unexpected sensitivity of the magnetism to the As z position [34]. We performed a series of calculations [35] for Ca, Sr and Ba 122 systems for FM, NN-AFM and SDW spin patterns using the experimental volume (ambient pressure, below T_N) both with $a = b$ and $a \neq b$ and optimizing the Fe-As distance (via As z position) for each case. Table 3 compares the Fe moments computed for the SDW pattern (the lowest-total-energy spin pattern among those considered) with the experimental values obtained using neutron diffraction and muon spin rotation (μ SR). In comparison to the situation in the 1111 systems, here for the 122 systems, the agreement between theory and experiment is seen to be better. However, the computed Fe magnetic moment is found to increase from Ca to Ba 122, whereas the trend is just the opposite according to the estimation of moments

from μ SR results. The moments obtained from neutron diffraction experiments are more reliable and remain rather constant for the three 122 systems considered here. The influence of the orthorhombic distortion on the calculated moments is quite negligible.

The better agreement between theory and experiment regarding the Fe magnetic moment in the case of 122 systems can be understood as follows. The computed *vs* measured magnetic moment discrepancy in the 1111 systems is usually explained to be a result of large spin fluctuations [36]. It is also known that spin fluctuation effects are reduced when going from 2D systems to 3D systems. Hence, the results presented in Table 3 provide additional support for the effective dimensionality considerations described above: the 122 systems have a more pronounced 3D nature than the 1111 systems. Since the description of spin fluctuation effects is insufficient in LSDA, the computed values are immune to such effects, while, of course, the values deduced from experiments do reflect these effects. Furthermore, since the Ba 122 system is more 2D-like than the Ca 122 system (*cf.* Table 2), it is expected to exhibit a smaller Fe moment (stronger spin fluctuation effects), and this is in agreement with the μ SR results.

Table 3. Comparison of the magnetic moments in μ_B per atom calculated using LSDA with the experimental values obtained via μ SR (a local probe) and neutron diffraction measurements. In LSDA, the moments were calculated for the SDW pattern for the Fe spins using a tetragonal lattice ($a = b$) and orthorhombic lattice ($a \neq b$). The Fe-As distance has been optimized for all the calculations reported in this table.

	LDA - SDW		μ SR	Neutron diffraction
	$a = b$	$a \neq b$		
Ca122	0.818	0.875	0.9 [37]	0.80 [38]
Sr122	1.1	1.13	0.8 [37]	0.94 [39]
Ba122	1.12	1.17	0.5 [37]	0.87 [40]

The interplay between the Fe-As distance and different magnetic long-range orders is illustrated in Fig. 4 for SrFe₂As₂. Similar results are found for the other 122 systems. The experimental value of the Fe-As distance in SrFe₂As₂ in the orthorhombic phase is reported to be 2.391 Å at 90 K [29]. Using the FM or the NN-AFM spin pattern produces a minimum in energy at around 2.31 Å along with a complete loss of the Fe magnetic moment. In the SDW pattern, the optimum value of the Fe-As distance is 2.327 Å, only slightly larger than that obtained using the FM or NN-AFM pattern, but the Fe magnetic moment is still 1.13 μ_B .

The As-*z* position is most likely one of the key issues for understanding of the iron pnictides. Present day density functional theory based calculations using LDA (described above) and also GGA [34, 41] are not able to reproduce all the experimental findings consistently. Since the magnetism and therefore the superconductivity crucially depends on this structural feature and the related accurate description of the Fe-As interaction, the improvement of the calculations in this respect may offer the key to the understanding of superconductivity in the whole family.

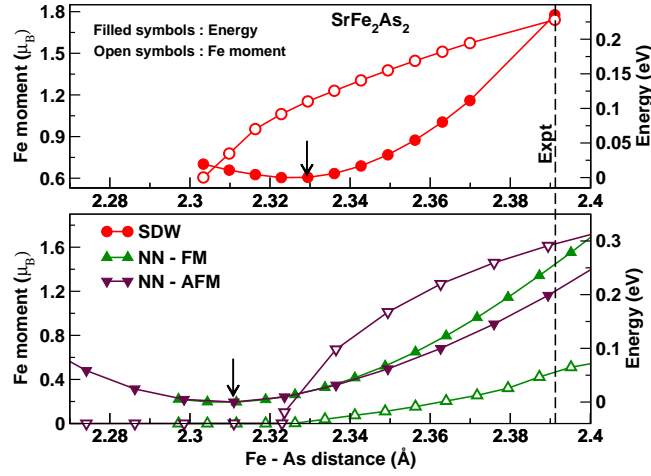


Figure 4. Energy and Fe magnetic moment as a function of the Fe-As distance using different spin patterns for $SrFe_2As_2$ at the experimental volume around 90 K [29]. Optimization using FM and NN-AFM pattern leads to a nonmagnetic solution, while the SDW pattern stabilizes with a Fe moment of $1.13 \mu_B$. The energy curves have been shifted by setting the minimum energy value to zero. The dashed vertical line refers to the experimental Fe-As distance obtained from Ref. [29]. The arrows indicate the position of the energy minima.

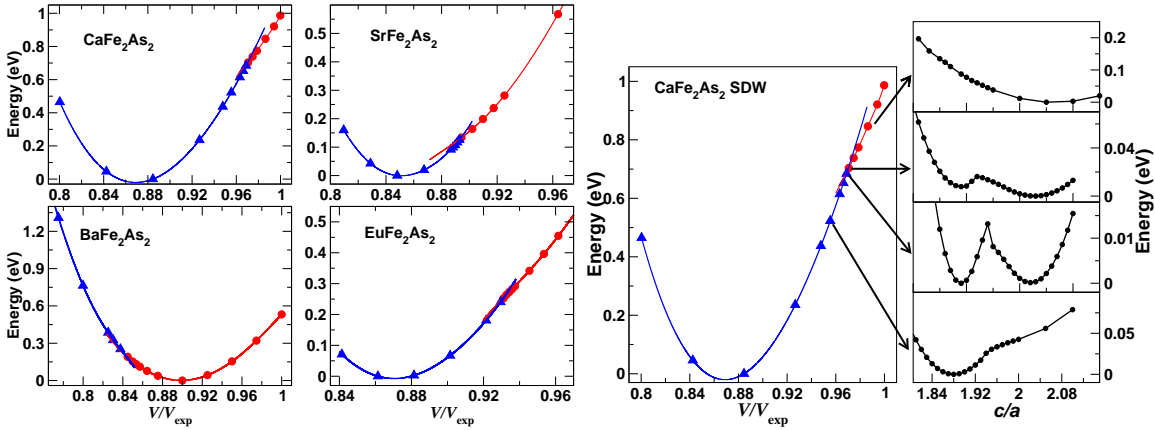


Figure 5. Left: Energy as a function of volume for AFe_2As_2 systems, with c/a ratio optimized. The two curves correspond to the antiferromagnetically ordered Fe spins in the SDW pattern with a non-zero moment (red circles) and zero moment (blue triangles). The kink at the intersection of these two curves is caused by a collapse of the c/a ratio upon pressure, which happens at the juncture when the systems lose their Fe moments and become non-magnetic. The c/a ratio collapse is most pronounced in $CaFe_2As_2$ due to the small size of the Ca ion and as the size of the A ions increases, this feature becomes more and more subtle. **Right:** The evolution of the c/a ratio collapse for $CaFe_2As_2$. Notice the emergence of the double minima.

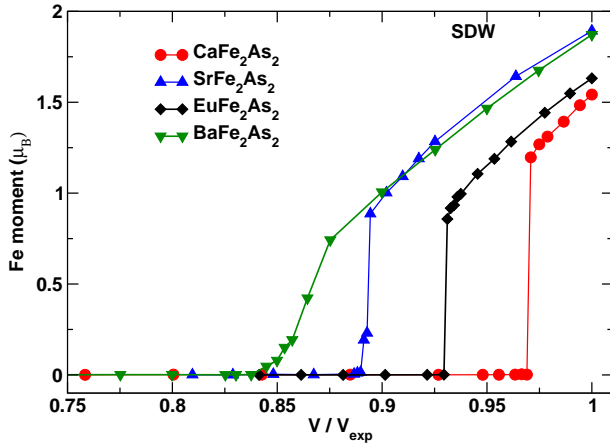


Figure 6. Volume dependence of the Fe moments corresponding to the energy-volume curves in Fig. 5. The quenching of the spin magnetic moment is highly abrupt for the compounds with pronounced c/a ratio collapse. The Fe moment in $BaFe_2As_2$ goes to zero smoothly reflecting the much smoother c/a variation obtained for this compound.

3.3. Effects of pressure

As mentioned above, superconductivity in the FeAs based systems can be achieved via doping of charge carriers. This kind of chemical substitution is quite convenient, but changes the electronic structure of the doped systems in a non-trivial way as compared to the undoped systems. Using external pressure as a probe on these systems creates a similar effect as doping, without the added complexity. Application of hydrostatic pressure suppresses both the tetragonal to orthorhombic distortion and the formation of the SDW, and leads to the onset of superconductivity in a similar fashion as charge doping. All the parent members of the 122 family have been reported to superconduct or show signs of its onset under pressure [42, 27, 17, 43, 44]. Ca122 was originally reported to superconduct ($T_c \approx 10$ K) at 0.4 GPa pressure [42, 27] but recent work by Yu and collaborators [45] do not observe any signature of bulk superconductivity and

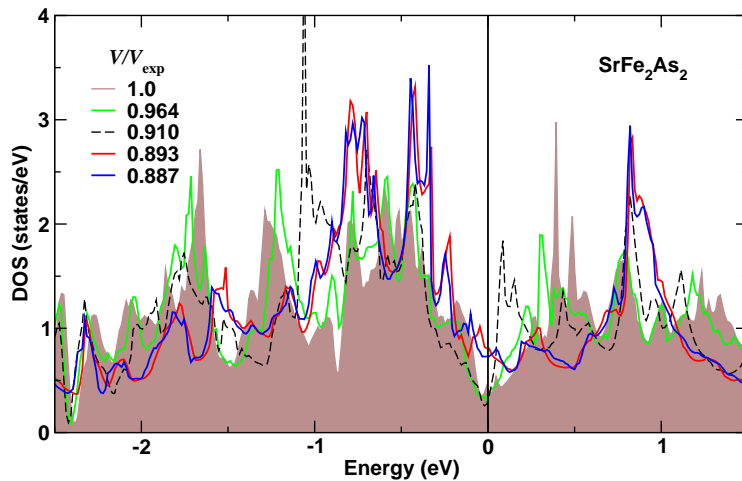


Figure 7. Total DOS per cell as a function of reduced volume for $SrFe_2As_2$ corresponding to the energy-volume curves in Fig. 5. In the SDW pattern, the total DOS for both the spin-up and spin-down channels are the same. Therefore, we show here the DOS from only one of the spin channels. The DOS at the Fermi level E_F at first decreases with decreasing volume, but later starts to increase after the Fe spin magnetic moment is quenched.

suggest a possible phase separation due to non-hydrostatic conditions. Similarly, Sr122 was first reported to superconduct at 2.8 GPa pressure with a T_c of 27 K [44], while on the contrary Kumar *et al.* [17] did not observe a zero-resistance state up to 3 GPa pressure. A sharp drop in resistivity above 2 GPa pressure was reported for Eu122, suggesting the onset of superconductivity and, more interestingly, signatures of possible re-entrant superconductivity. Though there exist conflicting reports of the transition pressure and possible phase separation in the sample under pressure, it is worthwhile to explore the evolution of the electronic structure and magnetism as a function of pressure. Pressure studies [27] on the CaFe₂As₂ system report a significant c/a collapse along with a structural transition (orthorhombic to tetragonal) under modest pressures of less than 0.4 GPa, while no such collapse has been reported for the other compounds. X-ray diffraction refinements carried out at 180 K for SrFe₂As₂ [17] observe an orthorhombic to tetragonal transition above 3.8 GPa, but no collapse of the c/a ratio is observed. Band structure calculations allow for the study of such features up to very large pressures, that might not be easily attainable through experiments. We have calculated energy as a function of volume for all the four systems in the 122 family. Firstly, we wanted to investigate the possibility of a c/a collapse for each member of the 122 family. Therefore, we calculated energy as a function of volume using the SDW pattern and optimizing only the c/a ratio at each volume. The internal As- z parameter was kept fixed at the experimental (room temperature) value. The results from these calculations are collected in Fig. 5. Surprisingly, all the four 122 systems have a kink in the energy-volume curve caused by a non-continuous change in the c/a ratio, which happens at the juncture when the systems lose their Fe moments and become non-magnetic (see Fig. 6). The sharpness of the kink is largest for Ca122 and decreases with the increasing size of the A ion. Such an A -ion size effect was also observed and discussed in section 3.2.1 when investigating the size of the orthorhombic b/a ratio. Our result obtained from LSDA (via a common tangent construction) for CaFe₂As₂ is in excellent agreement with the previously reported [27] experimental data, volume collapse: $\delta V^{\text{LDA}} \approx 4.7\%$, $\delta V^{\text{exp}} \approx 5\%$; ratio collapse: $\delta(c/a)^{\text{LDA}} \approx 9.8\%$, $\delta(c/a)^{\text{exp}} \approx 9.5\%$. Experimentally [27] a pressure of ~ 0.3 GPa induces a transition from the orthorhombic phase to a collapsed non-magnetic tetragonal phase for CaFe₂As₂. Scaling the volumes of the different 122 systems with respect to the experimental values (V/V_{exp}), one observes that the kink in the energy-volume curve for the other three 122 systems happens at lower volume ratios (or larger pressures) as compared to the Ca122. It should be worthwhile to investigate this structural feature experimentally by applying higher pressures to the Sr, Ba and Eu 122 systems.

Changes in the electronic structure as a function of reduced volumes were carefully monitored. Shown in Fig. 7 are the total DOS for SrFe₂As₂ at selected volumes. Similar results are obtained for other 122 systems. The DOS at E_F decreases gradually at first for up to 10% volume reduction with respect to the experimental volume. The Fe ions continue to carry a magnetic moment though the actual values are quite reduced. Upon further reduction of the volume, the spin moments get quenched and the DOS at E_F

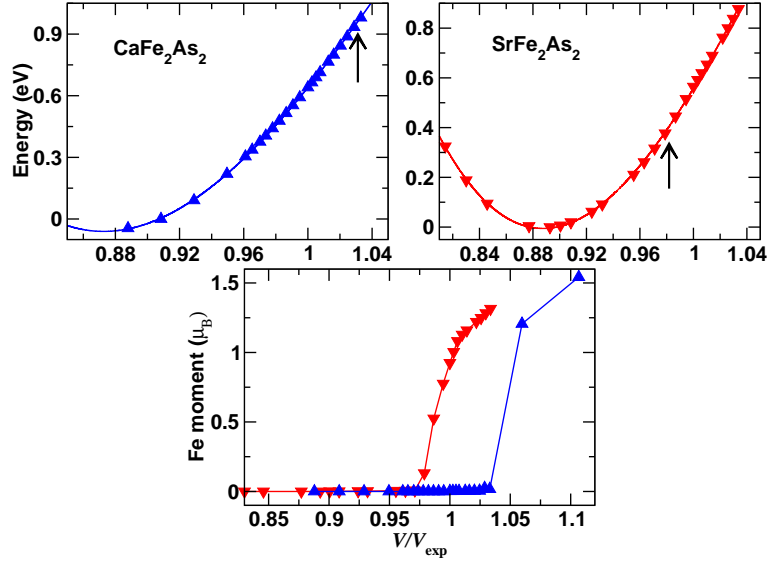


Figure 8. Top panel: Energy as a function of volume after a full relaxation of all the parameters for $SrFe_2As_2$ and $CaFe_2As_2$. Contrary to the results depicted in Fig. 5, we now no longer observe any kink at the juncture when the Fe ions lose the magnetic moment (corresponding data point is indicated using an arrow). **Bottom panel:** Fe magnetic moment as a function of volume for the Ca and Sr 122 systems. The results shown here are different from the moment values collected in Table. 3, because no c/a optimization was carried out for the latter.

begin to increase and the system becomes non-magnetic. At the experimental volume, the net moments on the various Fe orbitals are quite similar; with the $Fe-3d_{x^2-y^2}$ having a slightly larger value than the other orbitals. With the application of pressure, the net moments of all the five d orbitals decrease in a similar fashion and tend to zero.

Another important feature that needs to be addressed in regard to the energy-volume curves is the serious underestimation of the equilibrium volume within LDA. Generally, equilibrium volumes obtained from LDA are smaller within up to 8% of the experimentally reported values. In the case of 122 systems using SDW pattern, we obtain values that are 13%, 15%, 10%, and 13% smaller than the experimental reports for Ca, Sr, Ba and Eu 122 systems respectively. Moreover, at the LSDA equilibrium volume, contrary to the experimental reports, all the parent compounds are computed to be nonmagnetic. The reason for this discrepancy is unclear. In the previous sections we discussed the pronounced sensitivity of the Fe moments to the various structural parameters in these FeAs systems. Although with partial optimization (fixed As- z parameter) we have satisfactorily accounted for the experimentally observed c/a collapse in $CaFe_2As_2$, it is necessary to find out what the ultimate LSDA solution is regarding the geometrical structure and magnetism in the 122 systems. Consequently, for Ca and Sr 122 systems and using the SDW pattern, at each volume we have optimized all three free structural parameters in the following order: 1) As- z position, 2) c/a ratio, 3) b/a ratio. This sequence of steps has been repeated until the energies obtained are converged to an

accuracy of 10^{-6} eV. Collected in Fig. 8 are the energy-volume curves for the Ca and Sr 122 systems. The equilibrium volume obtained after a full optimization is only slightly larger than the values obtained after just a c/a optimization (see Fig. 5). Contrary to the results depicted in Fig. 5, we now no longer observe any kink at the juncture when the Fe ions lose their magnetic moments. The loss of moment for Sr122 is more gradual than for Ca122. As volume is decreased (higher pressures are applied) the Fe spin magnetic moments tend to zero while the orthorhombic distortion ratio b/a tends to unity so that at increased pressures the tetragonal lattice is favored. This observation of the lattice structure preferring the tetragonal symmetry when the Fe ions become nonmagnetic is consistent with our previous results in Sec. 3.2.1, and reaffirms the intimate connection between structure and magnetism for the 122 systems. Optimizing the As z parameter again tends to confirm certain experimental findings (the connection between SDW magnetic pattern and orthorhombic distortion) but not all (for example, lack of c/a collapse under pressure for $CaFe_2As_2$). This again re-affirms the need for a correct description of the Fe-As interplay to obtain consistent results.

3.4. Effects of charge doping

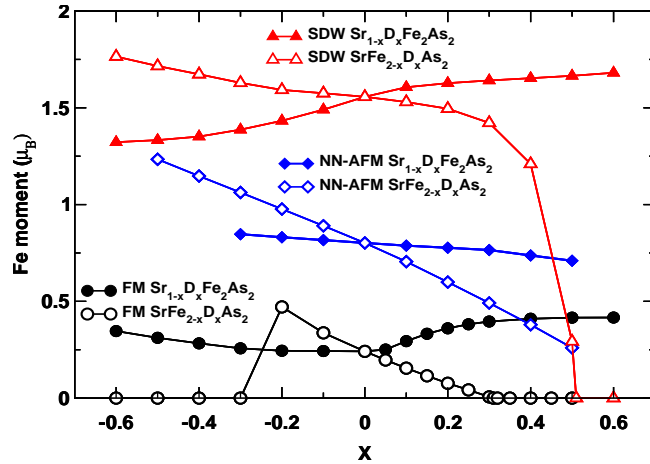


Figure 9. Results from the VCA calculations. Magnitude of the Fe moment as a function of charge doping (both on Sr site as well as Fe site) for different ordering patterns in $SrFe_2As_2$. When x is positive: electron doping; when x is negative: hole doping. The filled symbols and the open symbols indicate doping of the A site and the Fe site respectively. ‘D’ represents the dopant. Very different effects are observed when doping charge carriers on the Sr or Fe site. Magnetism is weakened when electrons are substituted on the Fe site, while strengthened when electrons are substituted on the Sr site. The relative trend between the different ordering patterns remains the same. We have used the experimental lattice parameters (at ≈ 300 K) and As- z value for all the calculations.

In order to understand the influence of charge doping (both electrons and holes) on the electronic structure and henceforth the magnetism, we performed total energy calculations using the VCA for three different spin patterns: FM, NN-AFM and SDW.

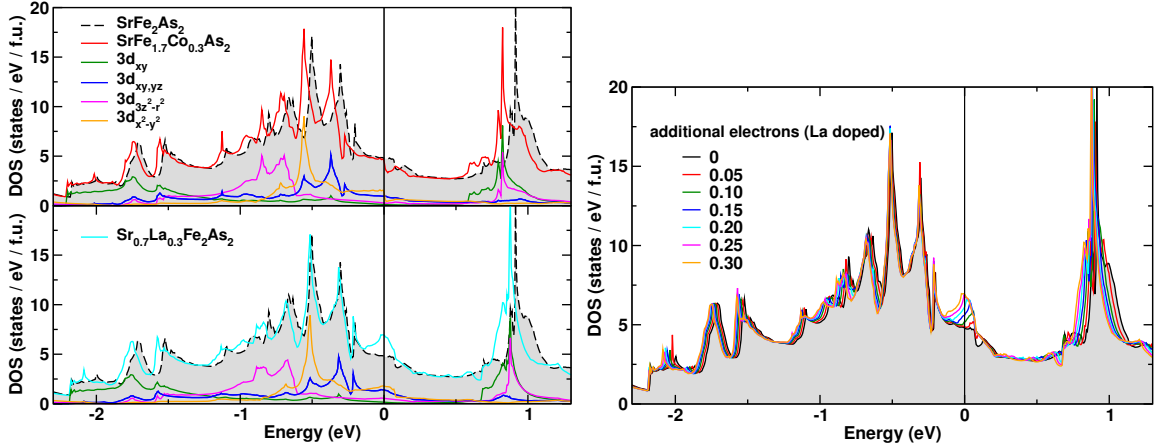


Figure 10. Top Left: Non magnetic total and Fe orbital resolved DOS from a VCA calculation for a 15% electron doping on the Fe site in Sr122. Upon electron doping, the DOS remains unchanged and displays a rigid-band-like behaviour. **Bottom Left:** Non-magnetic total and Fe orbital resolved DOS for a 30% electron doping on the Sr site in Sr122. Addition of electrons changes the shape of the DOS close to E_F drastically. A pronounced peak starts to appear close to E_F which tends to destabilize the system. The changes in the total DOS for various doping concentrations are shown in the right panel. **Right:** Non magnetic total DOS as a function of additional electrons on the Sr site in Sr122.

We considered both electron and hole doping on the A site as well as the Fe site. Our results for the changes in the Fe moment in SrFe_2As_2 are collected in Fig. 9. Similar results were obtained for other members of the 122 family. We observe very different effects depending on the sign (electrons or holes) and site (Sr or Fe) of the doping. Regardless of the choice of magnetic ordering, electron doping on the Fe (Sr) site weakens (enhances) the magnetism. This behaviour can be explained by analyzing how the nonmagnetic electronic structure changes with electron doping (see Fig. 10). Electron doping on the Fe site (left upper panel of Fig. 10) results in DOS very similar to that of the undoped case, main effect being the E_F moved toward higher energies to accommodate the added electrons. On the other hand, electron doping on the Sr site changes the resultant DOS drastically (see left lower and right panel of Fig. 10). Most of the major changes to DOS occur in the close vicinity of E_F giving rise to pronounced peaks at the E_F . A large value of DOS at the Fermi level, $N(E_F)$, is usually a sign of instability for an electronic system. The system can lower $N(E_F)$ by, for example, developing a long-range magnetic order provided the Stoner criterion is satisfied. The larger values of the computed Fe magnetic moments may reflect such an increased instability to magnetic order. Additionally, with reservations for possible thermodynamical considerations, appearance of this feature may explain why La doped 122 samples could not be synthesized until now.

Substitution of holes on the Sr site does not introduce significant changes to the Fe magnetic moment. Substitution of holes on the Fe site tends to enhance magnetism

for both AFM patterns whereas for the FM pattern the magnetism vanishes beyond a critical level of doping. However, this feature for the FM spin pattern is of no significance, because energetically it lies above both of the AFM patterns at all levels of doping.

3.5. Electric field gradient

Nuclear magnetic resonance (NMR) is a local probe that is extremely sensitive to certain details of the structure. Since the As z position is a key determinant of many of the electronic properties of the FeAs systems, the quadrupole frequency ν_Q from NMR measurements can provide a direct measure to the Fe-As interaction. Theoretically, ν_Q can be obtained by calculating the electric field gradient (EFG). The EFG is defined as the second partial derivative of the electronic potential $v(\vec{r})$ at the position of the nucleus

$$V_{ij} = \left(\partial_i \partial_j v(0) - \frac{1}{3} \Delta \delta_{ij} \right) \Delta v(0). \quad (1)$$

This traceless and symmetric tensor of rank 2 is described in the principal axis system by the main component V_{zz} and the asymmetry parameter $\eta = (V_{xx} - V_{yy})/V_{zz}$. V_{zz} is per definition the component with the largest magnitude $|V_{zz}| \geq |V_{yy}| \geq |V_{xx}|$ and is not necessarily parallel to the z -axis of the crystal. From these two parameters (V_{zz} and η) and the quadrupole moment for ⁷⁵As $Q = (0.314 \pm 0.006)$ b [46] the quadrupole frequency ν_Q for ⁷⁵As (with a nuclear spin of $I = 3/2$) can be calculated [47]

$$\nu_Q = \frac{eQV_{zz}}{2h} \sqrt{1 + \frac{\eta^2}{3}}. \quad (2)$$

The experimental lattice parameters, including the As z position for the calculation of the EFG for As in CaFe₂As₂, SrFe₂As₂ and BaFe₂As₂ were obtained from Ref. [27], [48], [12] respectively. For the parent compounds we investigated the influence of the As z position, the structural phase transition, the magnetism and the pressure on the EFG. We also investigated the effects of doping on the EFG.

First we focus on the As z dependence of the EFG. Just as the computed Fe magnetic moment, whose value show a strong dependence on the As z position (see Sec. 3.2.3), the EFG is also found to display a strong As z dependence. The EFG increases strongly for all three compounds, as the Fe-As distance decreases, see Fig. 11. In case of CaFe₂As₂, there is a minimum in the EFG for a displacement of roughly $\Delta z = -0.1$ Å from the experimental position, while for larger Fe-As distances the EFG increases again. The same trend is observed for the other two compounds, middle and lower panels in Fig. 11. They exhibit the minimum in the EFG at about $\Delta z = +0.05$ Å. For all the three parent compounds, the Fe-As distance at which the minimum in total energy occurs is smaller than that corresponds to the EFG minimum (see arrows in Fig. 11). For CaFe₂As₂ we observe a good agreement between the calculated EFG at the experimental As z position (for 250 K) and the measured EFG at 250 K [49] (the light green symbol in the upper panel of Fig. 11). In case of BaFe₂As₂ the magnitude of

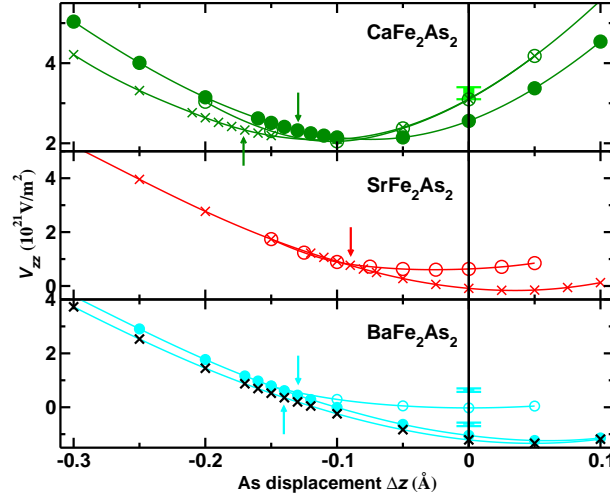


Figure 11. Dependence of the EFG for As on the As z position. $\Delta z = z - z_{\text{exp}}$. Different symbols show different calculations: cross = nonmagnetic with tetragonal symmetry, full circle = nonmagnetic with orthorhombic symmetry (almost identical to tetragonal symmetry for $SrFe_2As_2$ and therefore not shown) and empty circle = magnetic (SDW pattern) with orthorhombic symmetry. The total energy minimum is marked by an arrow for each nonmagnetic curve. The error bars show the experimental results for the tetragonal phase (at 250 K for $CaFe_2As_2$ and at 200 K for $BaFe_2As_2$ (the two error bars indicate the experimentally unknown sign of the EFG)).

the measured EFG at 200 K is roughly $0.7 \times 10^{21} \text{ V/m}^2$ [50], while the sign is unknown since it cannot be extracted from NQR measurements (In Fig. 11 the experimental EFG values with both signs are shown). The calculated V_{zz} for the experimental As z position is $-1.1 \times 10^{21} \text{ V/m}^2$. If the experimental EFG is negative, reasonable agreement between experiment and calculation is obtained. In a preliminary measurement for $SrFe_2As_2$ the quadrupole frequency ν_Q was determined to be positive and less than 2 MHz [51] and this is also consistent with the calculated EFG of 0.8 MHz at the experimental As z position. For members of the 1111 family; $LaFeAsO$ and $NdFeAsO$: the calculated EFG for the optimized As z position agreed better with the experimental EFG [52, 53]. Our results for three representative members of the 122 family as shown above follow a different trend: the calculated EFG using the experimental As z position agree better with the measured EFG values.

To study the influence of the orthorhombic distortion, but without the influence of magnetism we perform non-magnetic calculations both in tetragonal and orthorhombic symmetry. The orthorhombic splitting of the axes in the (a, b) plane has a rather small influence on the EFG. The EFG is larger for the orthorhombic symmetry for small Fe-As distances, i.e. $\Delta z < -0.1 \text{ \AA}$. In case of $SrFe_2As_2$, the effect of the orthorhombic splitting is so small, that the orthorhombic EFG curve in Fig. 11 is not shown (see middle panel of Fig. 11). In case of $BaFe_2As_2$, we observe similar behaviour as for $CaFe_2As_2$. The tetragonal and orthorhombic EFG curves cross close to the EFG minimum and the EFG is larger for the orthorhombic symmetry for smaller Fe-As distances, i.e. $\Delta z < +0.1 \text{ \AA}$.

Table 4. V_{zz} in 10^{21} V/m² for the nonmagnetic and different magnetic orders, all in orthorhombic phase.

compound	NM	FM	NN-AFM	SDW
CaFe ₂ As ₂	2.6	2.4	2.7	3.1
SrFe ₂ As ₂	0.2	0.3	0.2	-1.3
BaFe ₂ As ₂	-1.1	-1.0	-1.3	+1.3

For all three compounds we find that V_{zz} is parallel to the crystallographic z -axis for the non-magnetic calculations in both the tetragonal and orthorhombic symmetry.

Investigation of the influence of the magnetism on the EFG in the orthorhombic symmetry show that, FM or NN-AFM ordering of the Fe atoms does not change the EFG much, however, the SDW order has a huge influence on the EFG, *cf.* Table 4. For all the three systems, as the Fe-As distance is decreased, the magnetic moment is reduced and finally tends to zero. At this displacement value, the SDW EFG curves smoothly join the non-magnetic orthorhombic EFG curves as one would expect. In Fig. 11 the component of the EFG, that is parallel to the z -axis of the crystal is shown. As mentioned before, V_{zz} is found to be parallel to the crystallographic z -axis in all non-magnetic calculations. For the magnetic SDW phase the same behaviour is observed for CaFe₂As₂, but not for SrFe₂As₂ and BaFe₂As₂. For the latter two compounds, V_{zz} changes the axis, *i.e.*, the axis along which EFG is the largest changes as Fe-As distance is varied. For BaFe₂As₂, such a behaviour was also observed experimentally [50] when

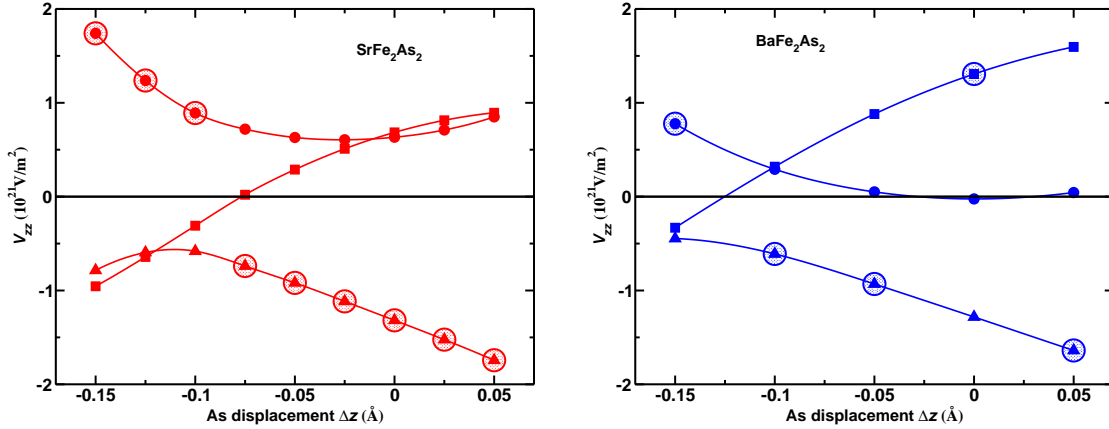


Figure 12. **Left:** The three components of the EFG tensor for SrFe₂As₂ in the orthorhombic SDW phase as a function of the As z position. $\Delta z = z - z_{\text{exp}}$. The component of the EFG, parallel to the crystallographic x -axis is shown by triangles up, the component parallel to the crystallographic y -axis by squares and the one parallel to the crystallographic z -axis by solid circles. V_{zz} , the largest one of these three, is marked by a large shaded circle for each As z position. **Right:** The three components of the EFG tensor for BaFe₂As₂ in the orthorhombic SDW phase as a function of the As z position. The rest of the notation is the same as the left panel.

going from the high-temperature nonmagnetic tetragonal phase to the low temperature SDW phase. Unfortunately for CaFe₂As₂, only the quadrupole frequency parallel, and not perpendicular to the crystallographic z -axis is provided in Ref. [49]. The three diagonal components of the EFG tensor V_{ii} , which are parallel to the x , y and z -axis of the crystal, vary continuously as a function of the As z position, as can be seen in Fig. 12. In case of SrFe₂As₂, V_{zz} is parallel to the x -axis for a displacement of As between $+0.05 \text{ \AA}$ and -0.075 \AA (which includes the experimental As z position) and parallel to the z -axis for a displacement between -0.1 \AA and -0.15 \AA . For BaFe₂As₂ according to its definition as the largest component V_{zz} fluctuates between all the three different axes (Fig. 12) In particular, at the experimental As z position V_{zz} is parallel to the y -axis. We also observe that the component parallel to the x -axis is very similar for both Sr and Ba 122 compounds. The components parallel to the y - and z -axis show the same variation with As z position, only the values for the two compounds are shifted by an almost constant amount. Fig. 3 in Ref. [49] shows the temperature dependence of the quadrupole frequency ν_Q for CaFe₂As₂: ν_Q increases drastically from 300 K to 170 K. At 170 K there is a large jump in the frequency due to the orthorhombic SDW phase transition. Between 170 K and 20 K ν_Q is rather constant. The calculated EFGs correspond to lattice parameters at 250 K and 50 K. For these two temperatures the quadrupole frequency (parallel to the crystallographic z -axis) is almost identical. This is in agreement with our result for the experimental As z position as seen in the upper panel of Fig. 11.

We also investigated the influence of pressure on the EFG. V_{zz} for different pressures was calculated for CaFe₂As₂ [50] and SrFe₂As₂ [17] using the experimental structural parameters reported as a function of pressure. Our result is shown in the inset of Fig. 13. In case of CaFe₂As₂, the EFG increases when the applied pressure is increased from 0 GPa to 0.24 GPa. For these pressures the structure is in the (orthorhombic) SDW phase. The next experimental pressure point is larger than the critical pressure of 0.3 GPa (Sec. 3.3), where the c/a collapse takes place. The structure changes into the nonmagnetic tetragonal phase and the calculated EFG increases drastically from roughly 3 to $10 \times 10^{21} \text{ V/m}^2$. Experimentally, the applied pressure for SrFe₂As₂ was much higher (up to 4 GPa) than for CaFe₂As₂, but no indications of a collapsed phase was found till now. Contrary to the jump in the calculated EFG at 0.3 GPa for CaFe₂As₂, EFG for SrFe₂As₂ increases monotonously without any kinks upto 4 GPa. It is worthwhile to measure the EFG for these systems to get a more clear picture.

Finally, the EFGs of the A site doped compounds were calculated with VCA. The validity of the VCA was checked by super cell calculations for SrFe₂As₂ and BaFe₂As₂. Due to the super cell construction, there are three different Wyckoff positions for As and hence three different EFGs, which lie reasonably close to the VCA EFG curve. In the VCA calculation we keep the structural parameters fixed for the different levels of doping. In Fig. 13 EFGs calculated in this manner are shown for CaFe₂As₂, SrFe₂As₂ and BaFe₂As₂. In case of CaFe₂As₂, the EFG increases when electrons are taken out and decreases when electrons are added to the system. This implies that the As electron

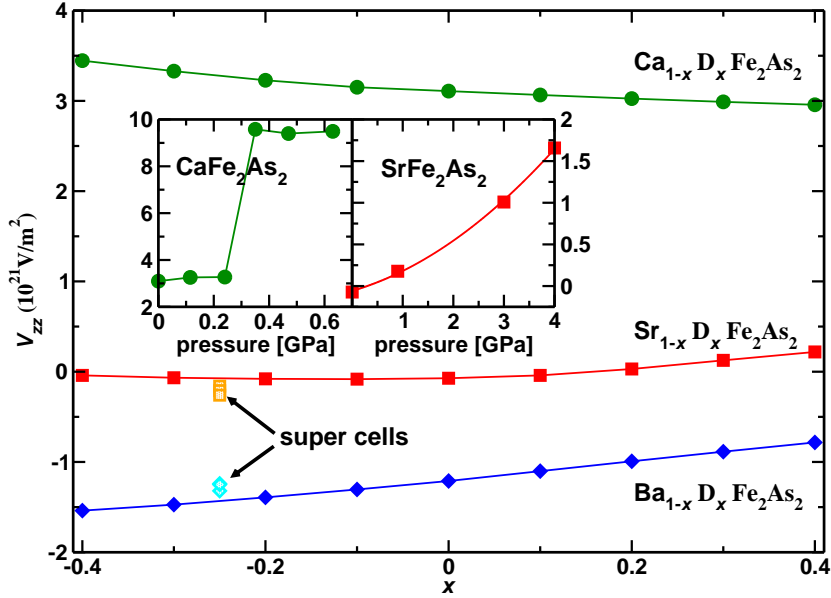


Figure 13. EFGs calculated for doped CaFe₂As₂ (green circles), SrFe₂As₂ (red squares) and BaFe₂As₂ (blue diamonds) using VCA. Results obtained from a four-fold super cell for $x = -0.25$ for SrFe₂As₂ (shaded orange squares) and BaFe₂As₂ (shaded blue diamonds) in the nonmagnetic tetragonal phase are also shown. **Inset:** Dependence of the EFG on pressure for CaFe₂As₂ (left) and SrFe₂As₂ (right). The latter is in the (nonmagnetic) tetragonal phase.

density gets more isotropic, when the system is electron doped. For BaFe₂As₂, the trend is the same as in CaFe₂As₂ whereas for SrFe₂As₂ the situation is slightly different: hole doping does not change the EFG much, while electron doping increases the EFG. Note however, that the calculated EFG for SrFe₂As₂ are quite small.

We conclude that the EFG in the 122 and in the 1111 systems behave similar [52, 53]: the effect of electron doping on the EFG is much smaller than the influence of the As z position and pressure (compare Fig. 11 and Fig. 13). This finding emphasizes again the crucial importance of a correct description of the Fe-As interaction (that is mostly responsible for the density around As) for the physical properties of the iron pnictides.

4. Results - Experiment

4.1. Substitutions of Fe by other 3d-metals

As already mentioned, at ambient pressure, no bulk superconductivity has been observed in stoichiometric $REOF_eAs$ and AFe_2As_2 ($A = Ca, Sr, Ba, Eu$) compositions (except for one report on SrFe₂As₂ crystals [54]). Instead, these parent compounds display the SDW transition at typically 100–200 K. A modification of the intralayer d_a^{Fe-Fe} and interlayer d_c^{Fe-Fe} distances and thus of the electronic states at E_F can be achieved by different means: (i) application of hydrostatic (or uniaxial) pressure, (ii) isovalent substitution of

a constituent atom by a smaller/larger ion in order to apply chemical pressure, (iii) hole doping or (iv) electron doping by non-isovalent substitution of any of the constituent atoms. The latter two methods usually also exert chemical pressure. Most excitingly, all these methods have been proven to be successful in generating bulk superconductivity in iron arsenide systems.

Application of pressure has widely been used to explore the phase diagrams of the superconducting chemical systems [42, 55, 44]. The method usually introduces no crystallographic disorder in the structural building units. In contrast when substituting a chemical constituent (methods ii–iv) always a certain degree of structural disorder is introduced. First, only substitutions on sites *in-between the Fe-As layers* were attempted. Based on the experience gained from extensive work on cuprates, such an indirect doping of the Fe-As layers is expected to introduce only minor structural disorder. In a localized (cuprate-like) as well as in an itinerant model of the arsenides, this type of doping amounts to a simple charge doping. Such experiments are therefore not suitable for discriminating between both models.

In contrast, a substitution of an atom species *within the Fe-As layer* can yield more information on the underlying physics. In an itinerant model the substitution of a small amount of Fe by another *d* element (*TM*) is expected to be similar to indirect doping since only the total count of electrons is relevant, i.e. a rigid-band picture should work in first approximation. In a picture with localized *d* electrons, on the other hand, doping on the Fe site should directly affect the correlations in the Fe-As layers. A behaviour drastically different from indirect doping should evolve. In cuprates the substitution of a few percent Ni or Zn on the Cu site leads to a strong reduction of T_c .

Therefore, several groups recently investigated the properties of solid solutions of the type $REO(\text{Fe}_{1-x}\text{Co}_x)\text{As}$ or $A\text{Fe}_{2-x}\text{Co}_x\text{As}_2$. Sefat *et al.* [56] and Wang *et al.* [57] first reported superconductivity in cobalt doped LaOFeAs with a maximum $T_c \approx 10$ K. Our group concentrated on the system $\text{SrFe}_{2-x}\text{TM}_x\text{As}_2$: while the pure Fe compound undergoes a lattice distortion and SDW ordering at $T_0 = 205$ K [11], Co substitution leads to a rapid decrease of T_0 , followed by the onset of bulk superconductivity in the concentration range $0.2 \leq x \leq 0.4$ [15]. The maximum T_c of ≈ 20 K is achieved for $x \approx 0.20$. This was in fact also the first observation of *electron-doping* induced superconductivity in $A\text{Fe}_2\text{As}_2$ compounds. Co substitution also generated bulk superconductivity with maximum $T_c \approx 22$ K in $\text{BaFe}_{2-x}\text{Co}_x\text{As}_2$ [16], however, the optimal doping seems to be lower than in the Sr system [58]. Substitution of the following *TM*, nickel, introducing twice as many electrons per atom into the Fe-As layer, also generates bulk superconductivity, albeit with lower T_c than Co substitution in the Sr compound [15]. However, for the corresponding Ba compound T_c up to 21 K is reported for $\text{BaFe}_{1.90}\text{Ni}_{0.10}\text{As}_2$ [59]. Only very recently another internal substitution, namely of As by P, was reported for EuFe_2As_2 [60] and LaOFeAs [61]. Also by this means the SDW transition can be influenced and superconductivity can be induced.

In Table 5 we present the lattice parameters and the SDW and superconducting transition temperatures (T_0 , T_c) of several $\text{SrFe}_{2-x}\text{TM}_x\text{As}_2$ solid solutions. Values for

T_0 can be most easily obtained from the corresponding anomaly in resistivity data (see Fig. 14). Besides Co and Ni substitutions in the Sr122 and Ba122 systems, no further d element substitutions have been reported yet. As demonstrated recently [15], substitution of Fe by Co suppresses rapidly T_0 (see Fig. 14). Bulk superconductivity, as proven by specific heat, magnetic shielding, and resistivity data, appears when $T_0 = 0$ or $T_0 < T_c$, which is reached for $x > 0.20$ [15]. Only about half of the substituting element ($x \approx 0.10$) is necessary to induce bulk superconductivity when using nickel [59]. Both elements then introduce 0.2 excess electrons into the FeAs layers. While the a lattice parameter does not change significantly with Co substitution the c lattice parameter decreases continuously in SrFe_{2-x}Co_xAs₂ [15] and with Ni content in BaFe_{2-x}Ni_xAs₂ [59]. Chemical homogeneity of the Co or Ni distribution is still an issue in current samples. One of the most important questions, the co-existence or mutual exclusion of SDW state and bulk superconductivity, has been discussed heavily for AFe₂As₂-based alloy series [62, 63, 64]. The answer is currently open and can be only given for really homogeneous samples.

Direct, in-plane *hole* doping might also induce superconductivity. Our new investigations show, that a substitution of Fe by Mn is possible and that it leads to a continuous increase of both the a and c lattice parameters with Mn content. Under these conditions a hole doping does not generate superconductivity. In contrast, in the indirectly-doped Sr_{1-x}K_xFe₂As₂ [4, 65] and Ba_{1-x}K_xFe₂As₂ [6] compounds the a lattice parameter decreases with x while c increases, keeping the unit cell volume almost constant. Also, the SDW transition temperature T_0 is suppressed with increasing Mn content in a different way (see Fig. 14) than for the Co and Ni substitutions where T_0 is suppressed for $x \approx 0.20$ and $x \approx 0.10$, respectively. Indeed, after an initial decrease of T_0 to ≈ 140 K for $x = 0.20$ the transition temperature seems not to decrease further with x . Thus, the doping with holes or electrons is not the only important factor for the appearance of superconductivity but a corresponding tuning of the distances $d_a^{\text{Fe-Fe}}$ and $d_c^{\text{Fe-Fe}}$ has to be accomplished also. At present, the microscopic origin of the differences upon Mn doping compared to Co or Ni doping is unclear. Therefore, further investigations for different substitutions are currently underway.

Magnetic susceptibility and specific heat data for polycrystalline samples SrFe_{2-x}Co_xAs₂ have already been presented [15]. Here, instead we report newer data obtained on two crystals with Co contents $x > 0.2$ grown by a flux method (see section 2.2).

Both crystals show strong diamagnetic signals in measurements after zero field cooling (ZFC). The onset temperatures T_c^{mag} are 17.8 K and 15.3 K, respectively. While the transition for crystal X1 is much wider than that of crystal X2 the T_c of the latter is somewhat lower, indicating a slightly larger Co-content in accordance with the EPMA investigations. The shielding signals (ZFC) corresponds to the whole sample volume, however the Meissner effect (FC) is very small. This is typical for Co-substituted AFe₂As₂ materials and probably due to strong flux line pinning. The random (and somewhat inhomogeneous) substitution of Fe by Co within the superconducting

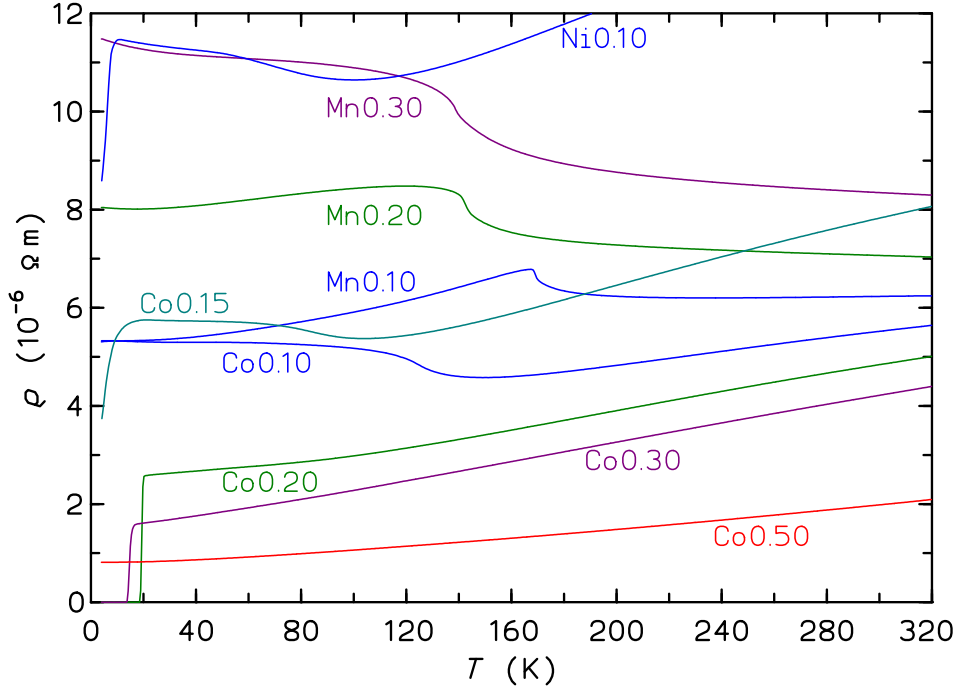


Figure 14. Electrical resistivity of polycrystalline $SrFe_{2-x}TM_xAs_2$ ($TM = Mn, Co, Ni$) samples

Table 5. Lattice parameters a, c of some $SrFe_{2-x}TM_xAs_2$ (nominal compositions) phase and superconducting transition temperature T_c^{mag} from magnetization measurements (onset, $T_{min} = 1.8 K$).

TM	x	a (Å)	c (Å)	T_c^{mag} (K)	T_0 (K)	Ref.
–	0.00	3.924(3)	12.38(1)	–	205	[11]
Co	0.10	3.9291(1)	12.3321(7)	–	130	[15]
	0.15	3.9272(1)	12.3123(5)	–	90	[15]
	0.20	3.9278(2)	12.3026(2)	19.2	< 30	[15]
	0.25	3.9296(2)	12.2925(9)	18.1	–	[15]
	0.30	3.9291(2)	12.2704(8)	13.2	–	[15]
	0.40	3.9293(1)	12.2711(7)	12.9	–	[15]
	0.50	3.9287(2)	12.2187(9)	–	–	[15]
	2.00	3.9618(1)	11.6378(6)	–	–	[15]
Ni	0.10	3.9299(1)	12.3238(6)	≈ 8	< 85	[15]
Mn	0.10	3.9319(2)	12.4161(7)	–	165	this work
	0.20	3.9384(3)	12.4615(23)	–	130	this work
	0.30	3.9441(2)	12.4832(7)	–	130	this work

layers seems to introduce effective pinning centers. This is a remarkable difference to superconducting compositions with substitutions outside the Fe-As layers.

As already demonstrated [15], the SDW ordering and the connected lattice distortion at $T_0 = 205$ K in SrFe₂As₂ [11, 29] is strongly suppressed by Co substitution, similar as for K substitution (indirect hole doping) [65]. For the two crystals no corresponding anomaly in $\rho(T)$ is observed.

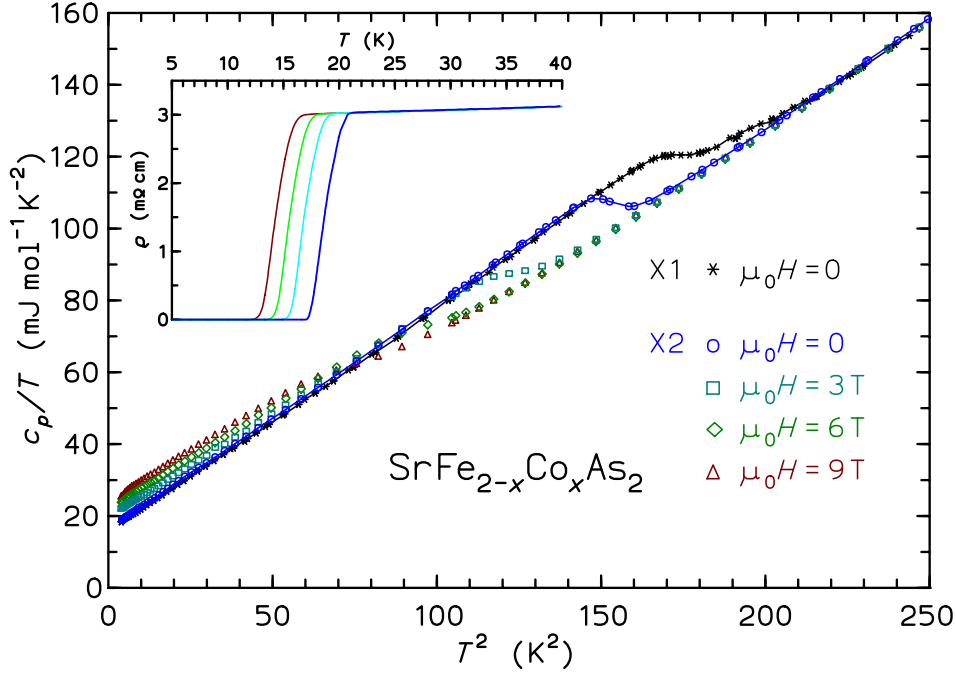


Figure 15. Molar isobaric specific heat c_p/T^2 of SrFe_{2-x}Co_xAs₂ crystal samples for different magnetic fields. For crystal X1 only data for $\mu_0 H = 0$ are given. Zero-field data points are connected by a line. The inset shows the resistivity of crystal X2 around T_c for $\mu_0 H = 0.01, 3, 6,$ and 9 T.

The specific heat $c_p(T)$ for the two crystals are shown in Fig. 15 in a $c_p(T)/T^2$ versus T representation. It can be clearly seen that crystal X1 has a very broad transition (with a “foot” at the high-temperature side) while crystal X2 displays a rounded but single-step anomaly. The specific heat jumps $\Delta c_p/T_c$ and the transition temperatures T_c^{cal} can be evaluated by a fit including a phonon background (harmonic lattice approximation) and an electronic term $c_{es}(T)$ according to the BCS theory ($\Delta c_p/T_c = 1.43\gamma$) or the phenomenological two-liquid model ($\Delta c_p/T_c = 2\gamma$, a model for stronger e-ph coupling). The inclusion of a residual linear term $\gamma'T$ was found to be absolutely necessary for a good fit.

$$c_p(T) = \gamma' T + \beta T^3 + \delta T^5 + c_{es}(T)$$

The jump at T_c is “broadened” in order to simulate the rounding of the transition steps due to chemical inhomogeneities. For the more homogeneous sample X2 no difference in the least-squares deviation is observed between the BCS and two-fluid model. We find for crystal X2 $\Delta c_p/T_c^{\text{cal}} \approx 12.0$ mJ mol⁻¹ K⁻² at $T_c^{\text{cal}} = 12.34$ K and also for crystal X1 similar values (≈ 12.5 mJ mol⁻¹ K⁻²; $T_c = 13.22$ K). Similar values of $\Delta c_p/T_c^{\text{cal}}$ were

observed in our previous study [15] of polycrystalline samples with Co-contents $x = 0.20$ and $x = 0.30$.

The existence of a linear specific heat term well below T_c is found for several $A\text{Fe}_2\text{As}_2$ -based alloys [15, 66]. For $H = 0$ we observe for both crystals values of γ' around $20 \text{ mJ mol}^{-1} \text{ K}^{-2}$. γ' generally increases with field. Whether the residual γ' is due to defects as in the case of early cuprate superconductor samples (see e.g. Ref. [67]) or whether it is an intrinsic contribution has to be clarified by further experiments. An intrinsic reason could be some ungapped parts of the Fermi surface [68]. For the specific heat jump $\Delta c_p/T_c$ in $\text{BaFe}_{2-x}\text{Co}_x\text{As}_2$ also relatively small values are reported ($\approx 25 \text{ mJ mol}^{-1} \text{ K}^{-2}$ [58]) while for $\text{Ba}_{0.6}\text{K}_{0.4}\text{Fe}_2\text{As}_2$ ($\Delta c_p/T_c \approx 100 \text{ mJ mol}^{-1} \text{ K}^{-2}$ [66, 62]) much larger jumps are observed. This may indicate that the superconducting Fermi surface portions in the Co-substituted compounds (in-plane doping) are strongly different from those in indirectly doped superconductors. Recent photoemission (ARPES) investigations indeed point out severe differences between (non-superconducting) $\text{BaFe}_{1.7}\text{Co}_{0.3}\text{As}_2$ and (superconducting) $\text{Ba}_{0.6}\text{K}_{0.4}\text{Fe}_2\text{As}_2$ [69]. In conclusion, our doping experiments on the Fe site strongly favor an itinerant picture over a localized scenario. Further thermodynamic and Fermi surface studies are required to resolve this issue.

5. Summary

In this paper, we presented a joint theoretical and experimental study of the systems $A\text{Fe}_2\text{As}_2$ ($A = \text{Ca, Sr, Ba, Eu}$) and $\text{SrFe}_{2-x}\text{TM}_x\text{As}_2$ ($\text{TM} = \text{Mn, Co, Ni}$) to investigate the relation of crystal structure and charge doping to magnetism and superconductivity in these compounds. Based on *ab-initio* electronic structure calculations we focused on the relationship between the crystal and electronic structure, charge doping and magnetism for the 122 family since their electronic structure and physical properties are quite similar to the other superconducting iron pnictide families (1111, 1111', 111, 11).

Although problems with an accurate description of the Fe-As interaction persist in present-day density functional calculations, this approach provides deep insight into many questions. We demonstrated that tetragonal to orthorhombic transition in the 122 compounds is intrinsically linked to the SDW formation in agreement with experimental observations. We find an anisotropic, pressure-induced volume collapse for $A\text{Fe}_2\text{As}_2$ ($A = \text{Ca, Sr, Ba, Eu}$) that goes along with the suppression of the SDW magnetic order. For $A = \text{Ca}$ our calculations are in excellent agreement with the experimental observations [27]. An experimental verification for the other compounds ($A = \text{Ca, Sr, Ba, Eu}$) would be desirable. With respect to the doping dependence in $\text{SrFe}_{2-x}\text{TM}_x\text{As}_2$, we find the correct trends compared to the experimental results. A more quantitative comparison will require the explicit treatment of the influence of the substitutional disorder on electronic structure and magnetism. This task is left for an extended future study.

As demonstrated also for the EFG, many properties of these compounds are sensitive to the As z position. Since the magnetism and therefore the superconductivity

crucially depend on this structural feature and the related accurate description of the Fe-As interaction, the improvement of the calculations in this respect may offer the key to the understanding of superconductivity in the whole family. In order to improve the present-day density functional calculation for this class of materials, the first step requires a deeper understanding of where, how and why these DFT calculation fail. Besides further calculational effort, a broader experimental basis, especially high pressure studies will be necessary to approach this complex issue.

Experimentally, we investigate the substitution of Fe in SrFe_{2-x}TM_xAs₂ by other 3d transition metals, TM = Mn, Co, Ni. In contrast to a partial substitution of Fe by Co or Ni (electron doping) a corresponding Mn partial substitution does not lead to the suppression of the antiferromagnetic order or the appearance of superconductivity.

The observed existence of a linear specific heat term in SrFe_{2-x}Co_xAs₂ well below T_c is extremely important for the understanding of the superconductivity in this compound and all related 122 superconductors with doping on the Fe site. Therefore, a careful investigation whether this feature is intrinsic or not is a crucial question. In order to answer it, further studies on carefully prepared and characterized high-quality samples are required. Since in many experiments a considerable sample dependence is observed, this issue is of large general importance for a future understanding of the superconducting iron pnictide materials.

We thank T. Vogel, R. Koban, K. Kreutziger, Yu. Prots, and R. Gumeniuk for assistance.

- [1] Kamihara Y, Watanabe T, Hirano M and Hosono H 2008 *J. Am. Chem. Soc.* **130** 3296–7
- [2] Ren Z A, Lu W, Yang J, Yi W, Shen X L, Li Z C, Che G C, Dong X L, Sun L L, Zhou F and Zhao Z X 2008 *Chin. Phys. Lett.* **25** 2215
- [3] Our nomenclature of “-x” means hypovalent substitution, while “x” means hypervalent substitution
- [4] Sasmal K, Lv B, Lorenz B, Guloy A M, Chen F, Xue Y and Chu C 2008 *Phys. Rev. Lett.* **101** 107007
- [5] Chen G F, Li Z, Li G, Hu W Z, Dong J, Zhang X D, Zheng P, Wang N L and Luo J L 2008 *Chin. Phys. Lett.* **25** 3403
- [6] Rotter M, Tegel M and Johrendt D 2008 *Phys. Rev. Lett.* **101** 107006
- [7] Wang X C, Liu Q Q, Lv Y X, Gao W B, Yang L X, Yu R C, Li F Y and Jin C Q 2008 arXiv:0806.4688v3
- [8] Mizuguchi Y, Tomioka F, Tsuda S, Yamaguchi T and Takano Y 2008 *Appl. Phys. Lett.* **93** 152505
- [9] Wu G, Xie Y L, Chen H, Zhong M, Liu R H, Shi B C, Li Q J, Wang X F, Wu T, Yan Y J, Ying J J and Chen X H 2008 arXiv:0811.0761v2
- [10] Ronning F, Klimczuk T, Bauer E D, Volz H and Thompson J D 2008 *J. Phys.: Condens. Matter* **20** 322201
- [11] Krellner C, Caroca-Canales N, Jesche A, Rosner H, Ormeci A and Geibel C 2008 *Phys. Rev. B* **78** R100504
- [12] Rotter M, Tegel M, Schellenberg I, Hermes W, Pöttgen R and Johrendt D 2008 *Phys. Rev. B* **78** R020503
- [13] Jeevan H S, Hossain Z, Kasinathan D, Rosner H, Geibel C and Gegenwart P 2008 *Phys. Rev. B* **78** 052501
- [14] Jeevan H S, Hossain Z, Kasinathan D, Rosner H, Geibel C and Gegenwart P 2008 *Phys. Rev. B* **78** 092406
- [15] Leithe-Jasper A, Schnelle W, Geibel C and Rosner H 2008 *Phys. Rev. Lett.* **101** 207004

- [16] Sefat A S, Jin R, McGuire M A, Sales B C, Singh D J and Mandrus D 2008 *Phys. Rev. Lett.* **101** 117004
- [17] Kumar M, Nicklas M, Jesche A, Caroca-Canales N, Schmitt M, Hanfland M, Kasinathan D, Schwarz U, Rosner H and Geibel C 2008 *Phys. Rev. B* **78** 184516
- [18] Koepfner K and Eschrig H 1999 *Phys. Rev. B* **59** 1743
- [19] Ophale I, Koepfner K and Eschrig H 1999 *Phys. Rev. B* **60** 14035
- [20] We used version 7.00 of the FPLO release for all calculations pertaining to structural and magnetic transitions, doping and pressure effects. For the calculation of the electric field gradient (EFG) version 5.19 was used. As basis set: Ca ($3s3p/4s4p3d+5s5p$), Sr ($3d4s4p/5s5p4d+6s6p$), Ba ($4d5s5p/6s6p5d+4f7s7p$), Fe ($3s3p/4s4p3d+5s5p$) and As ($3s3p3d/4s4p4d+5s5p$) were chosen for semicore/valence+polarization states. The high lying states improve the basis which is especially important for the calculation of the EFG.
- [21] Perdew J P and Wang Y 1992 *Phys. Rev. B* **45** 13244
- [22] Czyżyk M T and Sawatzky G A 1994 *Phys. Rev. B* **49** 14211
- [23] Anisimov V I, Zaanen J and Andersen O K 1991 *Phys. Rev. B* **44** 943
- [24] Liechtenstein A I, Anisimov V I and Zaanen J 1995 *Phys. Rev. B* **52** R5467
- [25] Morinaga R, Matan K, Suzuki H S and Sato T J 2008 arXiv:0809.3084v2
- [26] Bostrom M, Prots Y and Grin Y 2006 *J. Sol. State Chem.* **179** 2472
- [27] Kreyssig A, Green M A, Lee Y, Samolyuk G D, Zajdel P, Lynn J W, Bud'ko S L, Torikachvili M S, Ni N, Nandi S, Leao J, Poulton S J, Argyriou D N, Harmon B N, Canfield P C, McQueeney R J and Goldman A I 2008 *Phys. Rev. B* **78** 184517
- [28] Jesche A, Caroca-Canales N, Rosner H, Borrmann H, Ormeci A, Kasinathan D, Kaneko K, Klauss H H, Luetkens H, Khasanov R, Amato A, Hoser A, Krellner C and Geibel C 2008 *Phys. Rev. B* **78** R180504
- [29] Tegel M, Rotter M, Weiss V, Schappacher F M, Pöttgen R and Johrendt D 2008 *J. Phys.: Condens. Matter* **20** 452201
- [30] Ma C, Yang H, Tian H, Shi H, Lu J, Wang Z, Zeng L, Chen G, Wang N and Li J 2008 arXiv:0811.3270v2
- [31] Huang Q, Qiu Y, Bao W, Lynn J, Green M, Chen Y, Wu T, Wu G and Chen X 2008 *Phys. Rev. Lett.* **101** 257003
- [32] Wu G, Chen H, Wu T, Xie Y L, Yan Y J, Liu R H, Wang X F, Ying J J and Chen X H 2008 *J. Phys.: Condens. Matter* **20** 422201
- [33] Note that the structural parameters for FeSe are taken from a very old reference, and that plasma frequencies depend sensitively on the band structure, which in turn can be affected strongly by the details of the crystal structure.
- [34] Mazin I I, Johannes M D, Boeri L, Koepfner K and Singh D J 2008 *Phys. Rev. B* **78** 085104
- [35] Experimentally, the Eu spins in EuFe₂As₂ are shown to order anti-ferromagnetically in the $a - b$ plane. This in turn doubles the unit cell along the c -axis during the LDA+ U calculations and introduces to inequivalent As positions. Optimizing the Fe-As distance for this scenario is more time consuming and is therefore postponed.
- [36] Mazin I I and Johannes M D 2008 arXiv:0807.3737v1
- [37] Goko T, Aczel A A, Baggio-Saitovitch E, Bud'ko S L, Canfield P C, Carlo J P, Chen G F, Dai P, Hamann A C, Hu W Z, Kageyama H, Luke G M, Luo J L, Nachumi B, Ni N, Reznik D, Sanchez-Candela D R, Savici A T, Sikes K J, Wang N L, Wiebe C R, Williams T J, Yamamoto T, Yu W and Uemura Y J 2008 arXiv:0808.1425v1
- [38] Goldman A I *et al.* 2008 *Phys. Rev. B* **78** R100506
- [39] Zhao J *et al.* 2008 *Phys. Rev. B* **78** R140504
- [40] Matan K, Morinaga R, Iida K, and Sato T J 2008 arXiv:0810.4790
- [41] Yildirim T 2008 arXiv:0807.3936v2
- [42] Torikachvili M S, Bud'ko S L, Ni N and Canfield P C 2008 *Phys. Rev. Lett.* **101** 057006
- [43] Miclea C F, Nicklas M, Jeevan H S, Kasinathan D, Hossain Z, Rosner H, Gegenwart P, Geibel C

- and Steglich F 2008 arXiv:0808.2026v1
- [44] Alireza P L, Ko Y T C, Gillett J, Petrone C M, Cole J M, Lonzarich G G and Sebastian S E 2008 *J. Phys.: Condens. Matter* **21** 012208
- [45] Yu W, Aczel A A, Williams T J, Bud'ko S L, Ni N, Canfield P C and Luke G M 2008 arXiv:0811.2554v1
- [46] Pyykkö P 2001 *Mol. Phys.* **99** 1617
- [47] Abragam A 2006 *The principles of nuclear magnetism*, Oxford Univ. Press
- [48] Tetragonal phase: $a = 3.9250$, $c = 12.332$, $z(\text{As}) = 0.358$, orthrhombic pase: $a = 5.5819$, $b = 5.5197$, $c = 12.332$, $z(\text{As}) = 0.358$
- [49] Baek S H, Curro N J, Klimczuk T, Bauer E D, Ronning F and Thompson J D 2008 arXiv:0808.0744v3
- [50] Kitagawa K, Katayama N, Ohgushi K, Yoshida M and Takigawa M 2008 arXiv:0807.4613v3
- [51] Jeglič P private communication
- [52] Grafe H J, Lang G, Hammerath F, Paar D, Manthey K, Koch K, Rosner H, Curro N J, Behr G, Werner J, Leps N, Klingeler R and Bchner B 2008 arXiv:0811.4508
- [53] Jeglič P, Bos J W G, Zorko A, Brunelli M, Koch K, Rosner H, Margadonna S and Arčon D 2008 Submitted Phys. Rev. B
- [54] Saha S R, Butch N P, Kirshenbaum K and Paglione J 2008 arXiv:0811.3940v1
- [55] Park T, Park E, Lee H, Klimczuk T, Bauer E D, Ronning F and Thompson J D 2008 *J. Phys.: Condens. Matter* **20** 322204
- [56] Sefat A S *et al.* 2008 *Phys. Rev. B* **78** 104505
- [57] Cao G *et al.* 2008 arXiv:0807.1304v2
- [58] Tanatar M A, Ni N, Martin C, Gordon R T, Kim H, Kogan V G, Samolyuk G D, Bud'ko S L, Canfield P C and Prozorov R 2008 arXiv:0808.4991v1
- [59] Li L J, Wang Q B, Luo Y K, Chen H, Tao Q, Li Y K, Lin X, He M, Zhu Z W, Cao G H and Xu Z A 2008 arXiv:0809.2009v1
- [60] Ren Z, Tao Q, Jiang S, Feng C, Wang C, Dai J, Cao G and Xu Z 2008 arXiv:0811.2390v1
- [61] Wang C, Jiang S, Tao Q, Ren Z, Li Y, Li L, Feng C, Dai J and abd Zhu'an Xu G C 2008 arXiv:0811.3925v1
- [62] Rotter M, Tegel M, Schellenberg I, Schappacher F M, Pöttgen R, Deisenhofer J, Günther A, Schrettle F, Loidl A and Johrendt D 2008 arXiv:0812.2827v1
- [63] Chu J, Analytis J G, Kucharczyk C and Fisher I R 2008 arXiv:0811.2463v1
- [64] Wang X F, Wu T, Wu G, Liu R H, Chen H, Xie Y L and Chen X H 2008 arXiv:0811.2920v1
- [65] Chen G F *et al.* 2008 *Chin. Phys. Lett.* **25** 3403
- [66] Mu G, Luo H, Wang Z, Ren Z, Shan L, Ren C and Wen H 2008 arXiv:0812.1188v1
- [67] Triscone G and Junod A 1996 *Bismuth-based High-Temperature Superconductors* ed H Maeda and K Togano (Marcel Dekker, New York) pp 33–74
- [68] Drechsler S L *et al.* 2003 *Physica B* **329** 1352–4
- [69] Sekiba Y, Sato T, Nakayama K, Terashima K, Richard P, Bowen J H, Ding H, Xu Y M, Li L J, Cao G H, Xu Z A and Takahashi T 2008 arXiv:0812.4111v1